Observation of two-photon excitation-induced fluorescence of ground-state neutral carbon atoms in vacuum generated by laser ablation of graphite

Takashi Sakamoto [1] and Kosuke Yoshioka [1,2,*]

[1]*Department of Applied Physics, Graduate School of Engineering, The University of Tokyo, 7-3-1 Hongo, Bunkyo-ku, Tokyo 113-8656, Japan*
[2]*Photon Science Center, Graduate School of Engineering, The University of Tokyo, 2-11-16 Yayoi, Bunkyo-ku, Tokyo 113-8656, Japan*

(Received 16 September 2022; accepted 9 November 2022; published 29 November 2022)

We demonstrated a practical gas production method for the ground-state carbon atoms in vacuum by pulsed laser ablation of graphite. The observation of ^3P-^3D two-photon excitation-induced fluorescence at 165.7 nm in the absence of a visible ablation plume proved the production of ground-state carbon atoms and enabled the evaluation of the velocity distribution and atomic density of the produced gas. With a low ablation fluence of 0.18 J/cm^2 at 266 nm, the number of atoms produced was 1.5×10^8 per pulse. The temperature of the gas was approximately 5600 K. Spectral measurements of the plumes at higher excitation fluences of 8, 25, and 50 J/cm^2 indicated that thermal sublimation at a low excitation fluence was essential to produce ground-state carbon atom gases. This method provides a promising source of atomic gas of carbon for laser cooling and precision spectroscopy when combined with precooling, such as using buffer-gas cooling.

DOI: 10.1103/PhysRevA.106.052808

I. INTRODUCTION

Ultracold atoms, produced by laser cooling and trapping, are used as platforms for various applications, such as the observation of quantum degeneracy [1], quantum simulation [2], frequency standards [3,4], and ultracold collision studies [5]. Research on ultracold atoms of alkali and alkaline-earth metals has considerably progressed. However, laser cooling for atomic species of chemical and biological interest, including carbon and hydrogen, has not been realized. This is because the optically allowed electronic transitions from the ground state of these atoms lie in the vacuum ultraviolet (VUV) region, complicating the construction of light sources to drive effective cooling. As a classic example, a significant amount of effort was devoted to laser cooling of atomic hydrogen in a magnetic trap using one-photon [6,7] and two-photon excitations [8]. As an alternative method to approach atoms with transitions in the VUV region, laser cooling using a two-photon transition with a mode-locked laser has been proposed [9]; however, it has not been realized. This method has been demonstrated for rubidium using a two-photon transition enhanced by the near-resonant intermediate state with a mode-locked laser in the near infrared region [10]. However, it is experimentally difficult to apply this method to hydrogen and carbon [11], which do not have near-resonant intermediate states.

Moreover, a gas production method in vacuum for neutral carbon in the ground state with moderate vapor pressure has not been established. The sublimation temperature of carbon is high, e.g., approximately 3900 K for graphite. Thus, forming atomic vapor of carbon is more difficult compared with metals. In the previous studies on the formation of carbon atoms, Kokai and Koga used time-of-flight (TOF) mass spectrometry to detect neutral and ionic species produced by laser ablation of graphite in vacuum. They confirmed that a small number of neutral carbon atoms were present. They evaluated the velocity distribution of C_3 molecules and C^+ and C_3^+ ions [12]. However, no arrival time measurements for neutral carbon atoms were reported. In addition, the method cannot judge whether the detected neutral carbon atoms are in the ground state. Ong and Chang detected carbon atoms as emitting species from the emission spectral measurements of plumes produced by laser ablation of graphite in vacuum [13]. Das *et al.* demonstrated the formation of carbon atoms in the ground state via photolysis of carbon suboxide [14].

Spectroscopic measurements using two-photon excitation are effective means for probing carbon atoms in their ground state. The one-photon allowed transitions of carbon atoms lie in the VUV region and are difficult to excite. Conversely, two-photon transitions are accessible with light sources in the deep-ultraviolet region. In a previous study, Becker *et al.* detected ground-state carbon atoms in flames in low vacuum by monitoring the fluorescence around 143.5 nm associated with two-photon excitation at 287 nm (the $2s^22p^2\ ^3P$-$2s^22p3p\ ^3D$ transition) [15]. Aldén *et al.* performed two-photon excitation of carbon atoms at 280 nm (the $2s^22p^2\ ^3P$-$2s^22p3p\ ^3P$ transition) in flames at atmospheric pressure and low vacuum. They detected the ground-state carbon atoms through subsequent stimulated emission around 909 nm (the $2s^22p3p\ ^3P$-$2s^22p3s\ ^3P^o$ transition) [16]. The stimulated emission signal at approximately 909 nm after two-photon excitation at 280 nm was generated from the carbon atoms in laser-produced plasma in vacuum [17]. However, these spectroscopic measurements using two-photon excitation have not been utilized to investigate the atomic density and velocity distribution of ground-state carbon atoms produced in vacuum.

In this paper, we demonstrate the gas phase production of carbon atoms in the ground state (^3P) using laser

*yoshioka@fs.t.u-tokyo.ac.jp

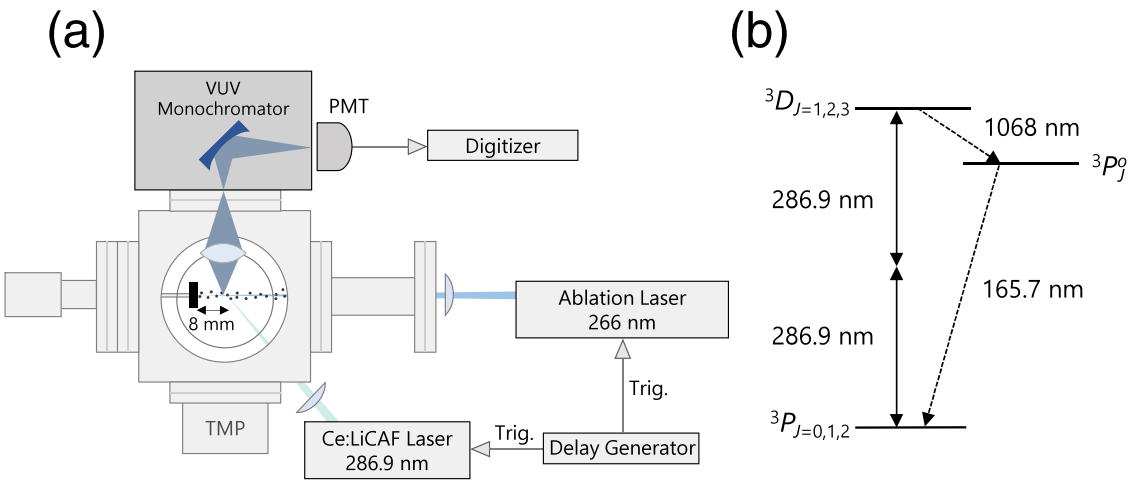

FIG. 1. (a) Experimental setup (TMP, turbo molecular pump; PMT, photomultiplier tube). (b) Schematic energy-level diagram of carbon considered in this paper.

ablation of graphite in vacuum and evaluate the properties of the produced atoms including the atomic density and velocity distribution, through the observation of two-photon excitation-induced fluorescence in the VUV region. The ^3P-^3D two-photon transition of neutral carbon was induced by a nanosecond pulsed laser at 286.9 nm. The detection of the subsequent fluorescence at 165.7 nm ($^3P^o$-^3P transition) proves the production of ground-state carbon atoms using laser ablation. TOF measurements using two-photon excitation-induced fluorescence enabled the evaluation of atomic density and velocity distribution. In addition, we show that there exists an appropriate fluence range of ablation lasers for the production of carbon atoms in the ground state based on the plume emission spectra. Moreover, we discuss a setup for preparing a low-temperature and dilute gas of carbon atoms with a specialized pulsed laser that could realize the laser cooling of carbon.

II. IDENTIFICATION OF THE GROUND-STATE CARBON ATOMS AND CHARACTERIZATION OF THE PRODUCED GAS

A. Experimental setup

Figure 1 shows the experimental setup and schematic energy-level diagram of carbon, showing the involved levels and transitions. Carbon atoms were produced by focusing 266-nm radiation from the fourth harmonic of a Q-switched Nd:YAG laser on a rotating highly oriented pyrolytic graphite (HOPG) target. The size of the target was $10 \times 10 \times 2$ mm. The ablation laser had a repetition rate of 10 Hz, pulse width of 4 ns, and maximum pulse energy of 5.5 mJ. The spot size of the ablation laser beam on the graphite sample was 1.5 mm in $1/e^2$ diameter. The produced particles including ions, molecules, and atoms were expanded in a vacuum chamber with a background pressure of 3×10^{-3} Pa.

Linearly polarized, nanosecond pulses from a homebuilt tunable Ce:LiCAF laser, pumped by the fourth harmonic of a Q-switched Nd:YAG laser, were used for the two-photon excitation. The laser wavelength was tuned to the two-photon resonance of the ^3P-^3D transition at 286.9 nm. The pulse duration was 2.5 ns, and the repetition rate was 10 Hz. The laser beam was focused into a spatial region at a distance of 8 mm from the target using a lens with a focal length of 100 mm, resulting in a peak intensity of 6×10^8 W/cm^2. The delay time between the ablation laser pulse and two-photon excitation was adjusted using a digital delay generator.

Two-photon excitation-induced fluorescence was detected to be perpendicular to both the excitation laser and the atomic beams. A 0.2-m monochromator equipped with a solar-blind photomultiplier tube (PMT) was used to detect the VUV signal. To improve the detection efficiency, a CaF_2 condenser lens was inserted into the vacuum chamber, yielding a solid angle of 0.67. The signal was recorded using a 10-bit digitizer with a sampling rate of 5 GS/s.

B. Experimental results and discussion

Figure 2 shows the temporal profile of the two-photon excitation-induced fluorescence of the ^3P-$^3P^o$ transition at 165.7 nm averaging over 3000 shots, together with a fitted curve. The horizontal axis represents the time since the irradiation of the Ce:LiCAF laser. In this setup, the pulse width of

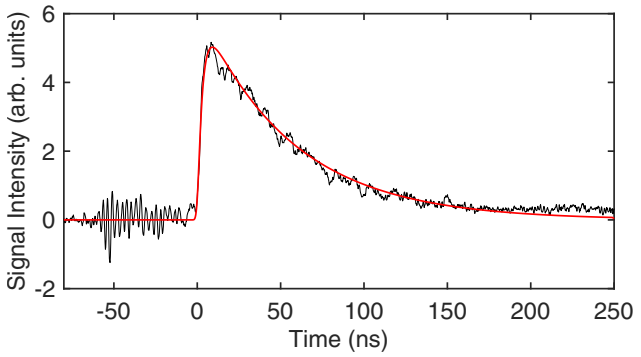

FIG. 2. Temporal profile of the two-photon excitation-induced fluorescence at 165.7 nm. The fluence of the ablation laser was 0.18 J/cm^2. The peak intensity of the excitation pulses was 6×10^8 W/cm^2. The red line is a fit to Eq. (1).

TABLE I. Dominantly contributing decay rates from the ^3D state to the $^3P^o$ state and from the $^3P^o$ state to the ^3P state [18].

Transition	A (10^6 s^{-1})
$^3D_3 \rightarrow {}^3P_2^o$	18.4
$^3D_2 \rightarrow {}^3P_1^o$	14
$^3P_2^o \rightarrow {}^3P_2$	261
$^3P_1^o \rightarrow {}^3P_0$	347

the Ce:LiCAF laser was significantly shorter than the lifetime of the two-photon excited state. It limited the average number of VUV photons emitted per two-photon excited atom to approximately 1. The fluence of the ablation pulse at 266 nm was 0.18 J/cm^2, where only blackbody radiation from the heated target surface was visible, and no bright emission from the plume was visible, as shown in Fig. 7. The delay between the ablation laser pulse and two-photon excitation was 2.5 μs. The peak intensity of the excitation pulses was 6×10^8 W/cm^2. Carbon atoms in the ground state are two-photon excited to the ^3D state by nanosecond pulses and undergo a two-step relaxation consisting of ^3D-$^3P^o$ transitions at approximately 1068 nm and the subsequent $^3P^o$-^3P transitions at approximately 166 nm. Therefore, the natural linewidth of the ^3D state is mainly determined by the ^3D-$^3P^o$ transition. Solving the rate equations of the three-level system assuming that the carbon atoms are excited to the ^3D state in advance, the expression for the temporal waveform of the fluorescence $S(t)$ is given by

$$S(t) = S_0(e^{-\gamma_1 t} - e^{-\gamma_2 t}), \tag{1}$$

where γ_1 and γ_2 are the decay rates from the ^3D state to the $^3P^o$ state and from the $^3P^o$ state to the ^3P state, respectively. S_0 is a constant. $\gamma_1 = 1.8 \times 10^7$ s^{-1} and $\gamma_2 = 3.5 \times 10^8$ s^{-1} are yielded by considering the temporal variation of the two-photon excitation rate and temporal resolution of the measurement, 2 ns, respectively. These decay rates are consistent with previously reported values. Table I shows the dominantly contributing decay rates among the six transitions from the ^3D state to the $^3P^o$ state and the six transitions from the $^3P^o$ state to the ^3P state [18].

The excitation intensity dependence of the fluorescence signal intensity at 165.7 nm was obtained to prove that the excitation process using the pulsed laser at 286.9 nm is a two-photon excitation. Figure 3 shows the intensity dependence of the two-photon excitation-induced fluorescence, where the relative signal intensity is plotted as a function of the square of the peak intensity of the excitation pulse at 286.9 nm. We changed the excitation intensity at 286.9 nm from 5×10^7 to 6×10^8 W/cm^2. The linear fit of the data showed that the fluorescence signal was proportional to the square of the peak intensity, indicating a two-photon excitation mechanism. No deviation from the square law was observed in the laser intensity range for this measurement, indicating that the excitation probability is in the perturbative regime.

The time constants of the time-resolved fluorescence signal at 165.7 nm in Fig. 2 and this excitation intensity dependence prove that the ground-state carbon atoms were produced in vacuum and that ^3P-^3D two-photon resonant excitation was performed.

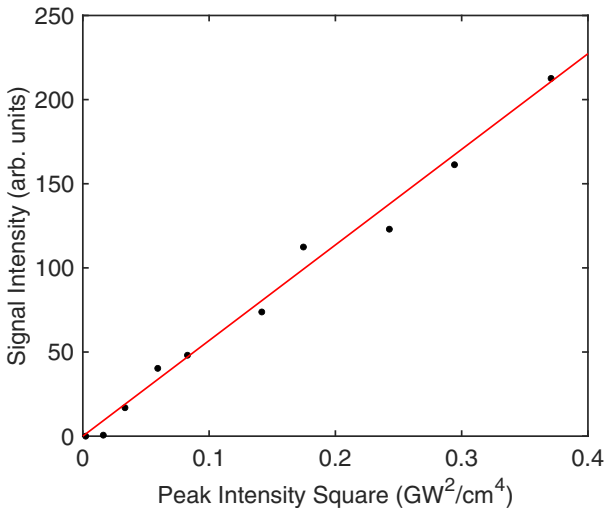

FIG. 3. Two-photon excitation-induced fluorescence intensity as a function of the square of peak intensity of the Ce:LiCAF laser (dots). The red line represents the linear fit.

We observed the fluorescence intensity at 165.7 nm while changing the time interval between the ablation laser pulse and the two-photon excitation pulse to evaluate the temperature of the atomic gas produced. The position of the focused 286.9-nm laser in the vacuum chamber was unchanged with respect to the measurement, as shown in Fig. 2. Figure 4 shows the arrival time distribution at a fluence of 0.18 J/cm^2, together with a fitted curve using a thermal Maxwell-Boltzmann distribution. The peak intensity of the Ce:LiCAF laser pulses was 6×10^8 W/cm^2.

The fraction of atoms that could be detected was limited by the ratio of the excitation pulse width of 2.5 ns to the spread of the arrival time of the generated atoms at the irradiated position. In addition, the volume of the two-photon excitation was significantly smaller than the spatial spread of the atomic cloud. Thus, in the current setup, approximately 10^{-3} of the total number of atoms produced interacted with the excitation

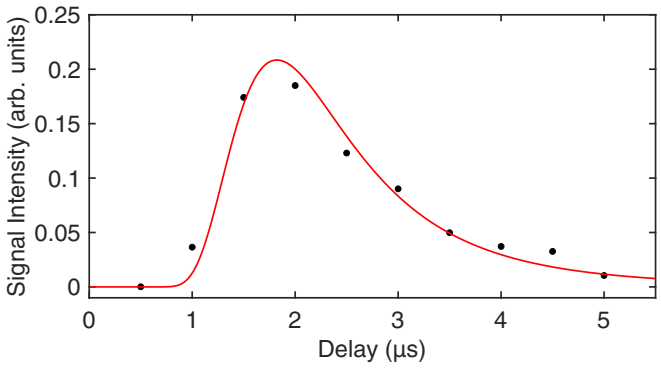

FIG. 4. Arrival time distribution of carbon atoms at a fluence of 0.18 J/cm^2 (dots). The red line represents a fit to a thermal Maxwell-Boltzmann distribution in an atomic beam with a temperature of 5600 K.

pulse. As discussed in Sec. II C, the two-photon excitation probability was approximately 10^{-2}. Therefore, the current experiment required a relatively long integration time (300 s) at each data point.

Assuming the Maxwell-Boltzmann distribution in an atomic beam, the relative signal intensity at t, $F(t)$, where t is the time interval between ablation and two-photon excitation, can be expressed as

$$F(t) = \frac{A}{t^5} \exp\left(-\frac{mL^2}{2k_B T t^2}\right), \tag{2}$$

where A is a constant, L is the distance from the surface of the HOPG sample to the position of two-photon excitation, m is the mass of the carbon atom, k_B is the Boltzmann constant, and T is the temperature of the produced gas. The details of the derivation of Eq. (2) are provided in Appendix A. We fitted the experimental data using this function to determine the gas temperature. The temperature of the gas was 5600 K, indicating that the most probable velocity was 3.4×10^3 m/s.

In a previous study, the relationship between the fluence of the ablation laser and the surface temperature of graphite was evaluated for the thermal ablation process using a pulsed laser at a wavelength of 532 nm with a pulse duration of 5 ns by establishing a temperature-dependent thermal diffusion equation [19]. If we adopted the maximum surface temperature (see Fig. 4) observed in Ref. [19] by only setting the laser fluence of the ablation pulse in the present experiment, the surface temperature could be less than 2000 K. This was several times lower than the gas temperature measured in Fig. 4. We assumed that this discrepancy originates from the difference in the wavelengths and pulse durations. The absorption length of HOPG is approximately three times shorter at 266 nm ($1/\alpha \approx 13$ nm) than at 532 nm ($1/\alpha \approx 40$ nm) [20]. In addition, our pulse duration was approximately 20% shorter than that in Ref. [19]. Therefore, a larger temperature increase is expected near the surface in the present experiment. This suggests that a nanosecond pulsed laser at 266 nm is beneficial for efficiently producing gas with a small heat inflow for buffer-gas cooling, which will be discussed in Sec. IV A. The two-photon transition probability of the ^3P - ^3D transition has to be determined to evaluate the atomic density of the produced atoms, which is discussed in the next section.

C. Two-photon transition probabilities and atomic density

1. Relation between signal intensity and atomic density

The atomic density of the produced atoms was estimated from the signal intensity of the two-photon excitation-induced fluorescence and two-photon transition probability to evaluate the effectiveness of gas production of carbon atoms by laser ablation. The relationship between the atomic density of carbon in the ground state n and the temporal profile of the two-photon excitation-induced fluorescence signal $S(t)$ can be expressed as

$$\int S(t)dt = s\eta N_{\mathrm{Exc}}, \tag{3}$$

$$N_{\mathrm{Exc}} = \alpha n V, \tag{4}$$

where s is the time integral of the PMT signal voltage corresponding to the emitted single photon, η is the collection efficiency of the emitted photons, N_{Exc} is the number of carbon atoms excited to the ^3D state in the observed region, V is the volume of the observed region, and α is the probability of two-photon excitation caused by the Ce:LiCAF laser pulse in the observed region.

s was derived as 30 mV ns from the single-shot measurement. η was estimated to be 1.1×10^{-3}, where we used 5.3×10^{-2} as the value of the solid angle of observation divided by 4π, 0.67 as the transmission of the CaF_2 condenser lens, 0.3 as the diffraction efficiency of the grating in the VUV monochromator, and 0.1 as the quantum efficiency of the PMT. Considering the beam size of the Ce:LiCAF laser and the geometry of the detection system, the observed region has a diameter of 200 μm and a height of 2 mm, with a corresponding volume V of 6.3×10^{-5} cm^3.

2. Effect of the temporal and spectral properties of excitation pulses

We evaluated the two-photon excitation probability α when the center frequency of the multimode laser pulse is resonant with a two-photon transition frequency. It is expressed as

$$\alpha = W\Delta t, \tag{5}$$

$$W = \frac{\sigma_0^2 G_2(0)}{\left(2\Delta\nu_L^2 + \Delta\nu_D^2 + \delta^2\right)^{1/2}} \left(\frac{I}{\hbar\omega}\right)^2, \tag{6}$$

where W is the two-photon excitation rate and Δt is the duration of the Ce:LiCAF laser pulse. σ_0^2 is the integrated two-photon absorption cross section with units of cm^4, which is a linewidth-independent quantity. $G_2(0)$ is the second-order correlation function of the Ce:LiCAF laser pulse when the delay is zero, which is introduced to deal with the temporal fluctuation of the laser intensity. Although we did not measure the value of $G_2(0)$, it is commonly assumed that $G_2(0) = 2$ for multimode lasers. The factor $(2\Delta\nu_L^2 + \Delta\nu_D^2 + \delta^2)^{-1/2}$ is introduced to account for the excitation inefficiency resulting from the finite linewidth of the absorption and excitation laser spectra, where $\Delta\nu_L$ is the linewidth of the Ce:LiCAF laser, $\Delta\nu_D$ is the Doppler width, and δ is the natural linewidth. I and $\hbar\omega$ are the peak intensity of the Ce:LiCAF laser pulse and photon energy at a wavelength of 286.9 nm, respectively.

3. Two-photon absorption cross section

According to Fermi's "golden rule," the expression of σ_0^2 is given by

$$\sigma_0^2(1 \to 2) = \frac{\omega^2}{4\epsilon_0^2 c^2} \left| \sum_i \frac{\mu_{2i}\mu_{i1}}{\hbar(\omega_{i1} - \omega)} \right|^2, \tag{7}$$

where μ_{ik} is the electric dipole matrix element between the i and k states. The summation is performed over all intermediate states, where dipole transitions between both the ground and excited states are allowed. To obtain the value of μ_{ik}, we use the Wigner-Eckart theorem, which is given by

$$\langle J_k, m_k | er_q | J_i, m_i \rangle = \frac{\langle J_i || er || J_k \rangle \langle J_k, m_k | J_i, m_i; 1, q \rangle}{\sqrt{2J_k + 1}}, \tag{8}$$

TABLE II. Calculated effective fine-structure cross sections for the $^3P_J \rightarrow {}^3D_{J'}$ two-photon transitions when the nine ground-state sublevels are equally populated (see text).

J	J'	σ_0^2 (cm^4)
0	1	0
0	2	5.0×10^{-37}
1	1	7.7×10^{-37}
1	2	4.9×10^{-37}
1	3	6.9×10^{-37}
2	1	2.1×10^{-37}
2	2	8.5×10^{-37}
2	3	1.4×10^{-36}

where $|J, m\rangle$ are the eigenstates of the total angular momentum J^2 and its z component J_z and $\langle J_k, m_k|J_i, m_i; 1, q\rangle$ is the Clebsch-Gordan coefficient. r_q is the qth component of the spherical tensor operator of rank 1, and $q = 0\,(\Delta m = 0)$ when using a linearly polarized laser. $\langle J_i||er||J_k\rangle$ is a reduced matrix element that does not depend on m, m', or q. The reduced matrix element can be derived from the Einstein A coefficient using the following relationship:

$$A_{ki} = \frac{1}{2J_k + 1} \frac{16\pi^3 \nu_{ki}^3}{3\epsilon_0 hc^3} |\langle J_i||er||J_k\rangle|^2. \tag{9}$$

For example, the reduced matrix element $|\langle {}^3D_3||er||{}^3P_2^o\rangle|$ is calculated to be 7.47×10^{-29} C m using 1.84×10^7 s^{-1} as the value of the Einstein A coefficient. Table II lists the calculated two-photon absorption cross sections σ_0^2 between the ^3P_J and $^3D_{J'}$ states, where we considered only the $^3P^o$ states as intermediate states because of their dominant contribution to the cross sections. The change in the two-photon absorption cross section is only approximately 5%, even if states up to the $^3D^o$ state are considered, which is the next dominant intermediate state after the $^3P^o$ state. For simplicity, we defined the sum of the cross sections over m as the effective cross section, which is given by

$$\sigma_0^2(J \rightarrow J') = \sum_m p_{J,m} \sigma_0^2(|J, m\rangle \rightarrow |J', m\rangle), \tag{10}$$

where $p_{J,m}$ is the occupancy of the $|J, m\rangle$ state. The largest frequency interval between the nine magnetic sublevels of the ground state is approximately 1.3 THz (the corresponding temperature of 62 K), whereas the temperature of the produced gas is several thousand Kelvin. Therefore, each magnetic sublevel is equally occupied, and we can use the value of $p_{J,m}$ to be 1/9.

In the present experiment, the excitation laser was predominantly resonant with the $^3P_{J=2} \rightarrow {}^3D_{J'=3}$ transition, and other transitions were neglected. In this case, σ_0^2 is 1.4×10^{-36} cm^4. To evaluate the line-shape factor, we used the value of $\Delta\nu_L$ as 300 GHz, $\Delta\nu_D$ as 20 GHz, and δ as 18 MHz. The pulse duration Δt was 2.5 ns, and the laser intensity I was 6×10^8 W/cm^2. Finally, the two-photon excitation probability α was evaluated to be 1.2×10^{-2}.

4. Evaluation of the density and number of atoms

We evaluated the atomic density at 2.5 μs in the region of detection (i.e., 8 mm away from the graphite target). The maximum atomic density $n = N_{\mathrm{Exc}}/\alpha V = 6 \times 10^9$ cm^{-3} when the laser fluence of gas production is 0.18 J/cm^2. For comparison, the saturation vapor pressure of rubidium at 100 °C in typical laser-cooling experiments corresponds to an atomic density of 2×10^{13} cm^{-3}. We further evaluated the total number of ground-state carbon atoms N produced per ablation pulse to be 1.5×10^8 using the derived atomic density assuming that the produced atoms travel along the sample normal (see Appendix B).

III. INVESTIGATION OF EMISSION SPECTRA AT VARIOUS FLUENCES OF THE ABLATION LASER

A. Time-resolved measurement of the background emissions in the VUV region under intense ablation

From the perspective of atomic spectroscopy and generation of cold atoms, a larger number of atoms is favorable. We studied the ablation fluence dependence of the characteristics of the generated particles to investigate the possibility of further increasing the number of atoms produced by laser ablation. For fluences lower than 0.18 J/cm^2, the reproducibility of the signal intensity could not be ensured for long-time measurements of several hours, presumably because the physical state of the target surface changed gradually. Here, we increased the ablation fluence by increasing the pulse energy at 266 nm. In this case, we observed the ablation plume glowing in the visible wavelength region when the fluence reached approximately 0.3 J/cm^2. Moreover, we found that spontaneous emission at 165.7 nm occurred when the ablation plume was visible, under no resonant two-photon excitation. This implies that the thermal energy of the carbon atoms significantly increased.

We reconfigured the detection apparatus to detect and conduct time-resolved measurements of the VUV photons that are emitted approximately 20 cm away from the HOPG sample to evaluate the velocity of the carbon atoms using the VUV emission at 165.7 nm. The spot size of the ablation laser beam was changed on the graphite sample to 120 μm in $1/e^2$ diameter to obtain higher fluences. In this setup, we placed a bandpass filter in the VUV range in front of the PMT instead of the VUV monochromator. Therefore, VUV photons at 156 nm associated with the $^3D^o$-^3P transition may also be detected. The bandpass filter and PMT were purged with nitrogen.

Figure 5 shows the temporal profiles of the background VUV emissions at fluences of (a) 8 J/cm^2, (b) 25 J/cm^2, and (c) 50 J/cm^2 with a schematic diagram of the reconfigured setup [Fig. 5(d)]. Carbon atoms were produced at $t = 0$. Signal peaks can be observed at (a) 7.8 μs, (b) 5.5 μs, and (c) 3.9 μs. These signals originate from the spontaneous emission of excited carbon atoms in the $^3P^o$ state, reaching the detected volume in the vacuum chamber. The $^3P^o$-^3P transition at 165.7 nm occurs within several nanoseconds, and this can be found near the zero delay in Fig. 5 as stray light originating from positions near the surface that scatters in the vacuum chamber [see Fig. 5(d) for the detection field of view]. Therefore, the signal at the microsecond timescale is a

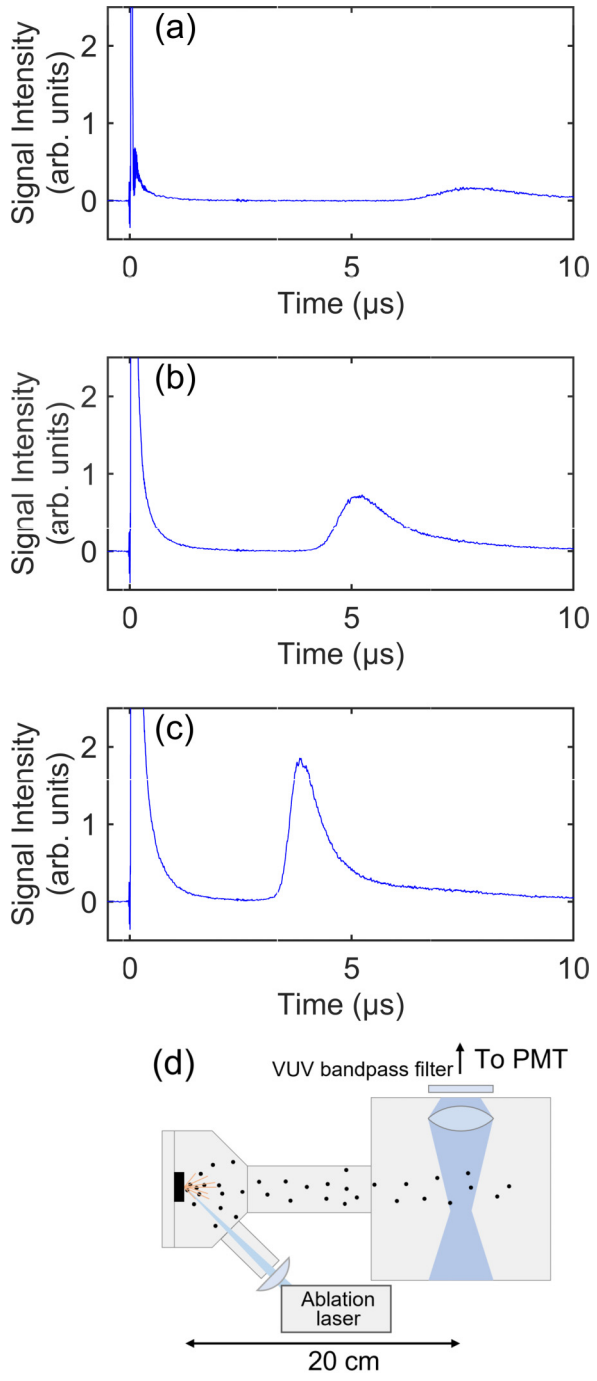

FIG. 5. Background VUV emissions from carbon atoms passing through the observed volume in vacuum 20 cm away from the HOPG sample at fluences of (a) 8 J/cm^2, (b) 25 J/cm^2, and (c) 50 J/cm^2. (d) Schematic of the experimental setup. The shaded area is the detection field of view.

consequence of slow decay channels from the higher excited states to the $^3P^o$ and $^3D^o$ state that eventually decay to the ground state emitting VUV photons at 165.7 and 156.0 nm, respectively (see Fig. 6). The equivalent velocities of the atoms are approximately (a) 2.6×10^4 m/s, (b) 3.6×10^4 m/s, and (c) 5.1×10^4 m/s. These velocities are at least eight times faster than the velocity obtained with two-photon excitation during ablation under conditions where no bright emission from the plume is observed. The velocity distributions cannot be fitted by thermal Maxwell-Boltzmann distributions.

B. Emission spectrum of the plume in the visible region under intense ablation

We measured the time-integrated emission spectrum of the plume in the visible wavelength region to spectroscopically investigate the particles produced in the ablation plume observed at high fluences. A grating monochromator with a cooled Si CCD image sensor was used to obtain the emission spectrum. The observed wavelength range was 425–520 nm. Figure 6 shows the emission spectra of the plume at fluences of (a) 8 J/cm^2, (b) 25 J/cm^2, and (c) 50 J/cm^2 in addition to the identification of prominent spectral lines.

At a fluence of 8 J/cm^2, the emission lines because of the Swan bands of the C_2 molecules were dominant; no signals were observed from other emitting species. Prominent emission lines originated from neutral carbon atoms, and emissions from monovalent carbon ions were also observed when we increased the fluence to 25 J/cm^2. Conversely, when we increased the fluence to 50 J/cm^2, the emission from monovalent carbon ions became more prominent, and the emission from C_2 molecules was no longer observed.

Emission spectral measurements in the visible region indicated that neutral carbon was efficiently produced at a fluence of 25 J/cm^2. In contrast, the observed visible emission corresponded to transitions between high-energy excited states, as shown in Fig. 6(d). These transitions have long lifetimes of the order of microseconds (e.g., 2.9 μs for the $2s^2 2p4p\,^3P_1$-$2s^2 2p3s\,^3P^o_0$ transition at 476.23 nm). Therefore, carbon atoms with visible emission traveled tens of centimeters before the $^3P^o$-^3P and $^3D^o$-^3P transitions at 165.7 and 156.0 nm, which were responsible for the background VUV emission signal. Highly excited carbons that have long relaxation times to the ground states and travel at high velocities are unsuitable for fine laser spectroscopy and cold atom experiments, such as laser cooling and trapping.

C. Emission spectrum in the vicinity of the HOPG target in the visible region under relatively weak ablation

For comparison, we measured the emission spectrum of the plume at a fluence of 0.18 J/cm^2, where two-photon excitation-induced fluorescence was observed. The bright plume was visible at all fluences listed in Sec. III B. However, the emission in the vicinity of the graphite surface at a fluence of 0.18 J/cm^2 was too weak to visually detect a plume. To obtain clear signals, we placed the focusing lens close to the HOPG sample and extended the integration time in signal acquisition from 20 to 120 s. Figure 7 shows the emission spectra of the plume at a fluence of 0.18 J/cm^2 in the wavelength ranges of (a) 425–520 nm and (b) 400–800 nm.

At a fluence of 0.18 J/cm^2, no prominent peaks corresponding to the electronic transitions of the produced particles were observed, except for the Swan bands (see Fig. 6), which appeared weakly on a continuous background signal. These results, combined with the fact that no VUV emission was observed solely by irradiating the ablation laser pulse, indicate that there was no laser-induced plume near the surface, and neutral carbon atoms were not produced in the excited state.

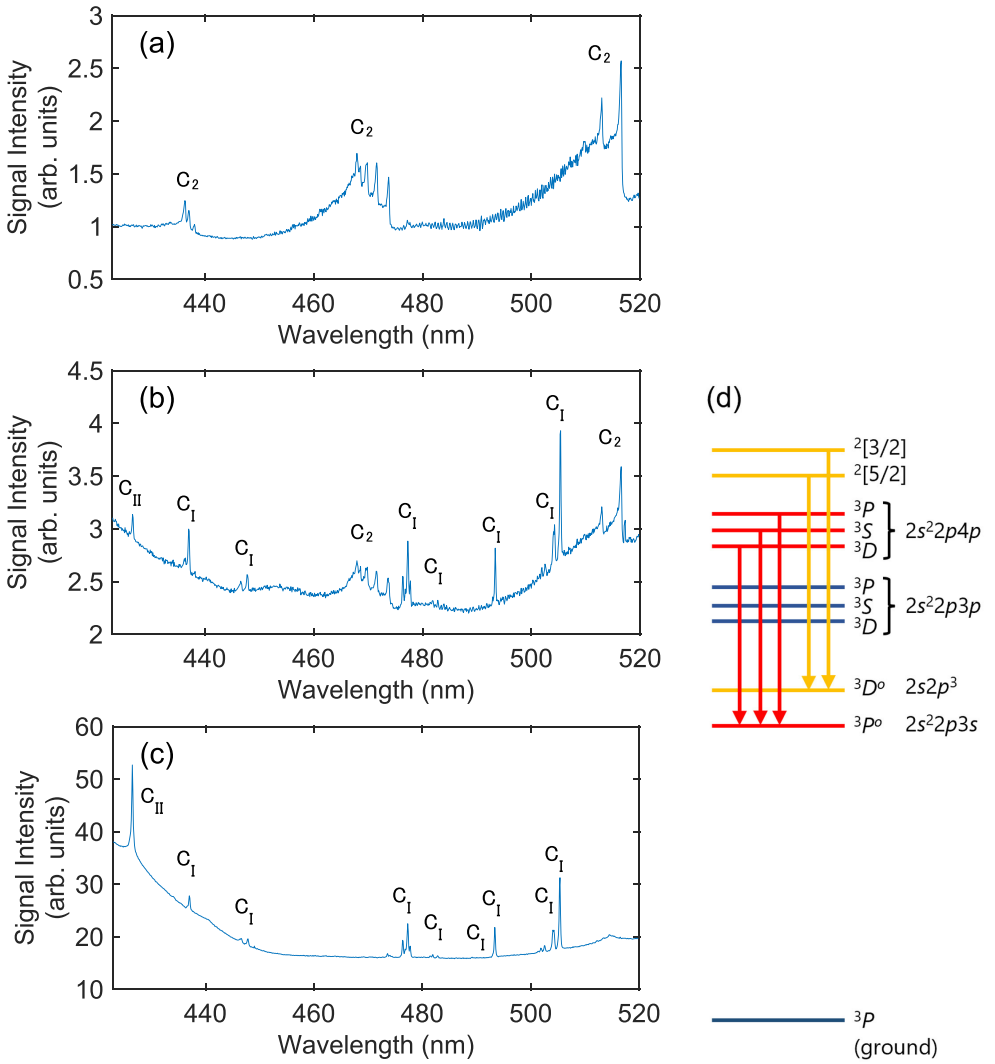

FIG. 6. Emission spectrum of the plume at fluences of (a) 8 J/cm^2, (b) 25 J/cm^2, and (c) 50 J/cm^2. C_2, C_I, and C_{II} indicate that they originate from molecules, neutral atoms, and singly ionized monoatomic ions, respectively. (d) Examples of the electronic transitions corresponding to visible emission of carbon. The red arrows indicate transitions between excited states that eventually lead to the $^3P^o$-^3P transition at 165.7 nm. The $2s^22p4p\ ^3P_1$-$2s^22p3s\ ^3P_0^o$ transition at 476.23 nm is one of the strongest of these transitions. The yellow arrows indicate examples of transitions between excited states leading to the $^3D^o$-^3P transition at 156.0 nm. The $2s^22p5f\ ^2[7/2]_4$-$2s2p^3\ ^3D_3^o$ and $2s^22p4f\ ^2[5/2]_3$-$2s2p^3\ ^3D_2^o$ transitions are located at 446.65 and 504.18 nm, respectively.

Moreover, the velocity distribution of the produced carbon atoms was fitted well with a thermal Maxwell-Boltzmann distribution (see Fig. 4). Therefore, the ground-state neutral carbon atoms were produced presumably because of thermal sublimation rather than other processes such as collision-induced dissociation in a laser-induced plume or nonthermal process, as observed in laser ablation using femtosecond pulses. In the wavelength range of 400–800 nm, broadband emission corresponding to blackbody radiation from the heated target was observed during laser irradiation, and no prominent peaks were observed except for the peak at 532 nm, due to the second-order diffraction of the ablation laser at 266 nm.

The results of this paper indicate that relatively low-temperature thermal sublimation that does not accompany electronic excitation is essential for preparing a gas of carbon atoms in the ground state using a graphite sample and laser ablation. As we observed VUV emission at a fluence of 8 J/cm^2, where only the Swan bands appear in the visible region, we recommend monitoring the VUV emission to avoid excessive heating of the surface of the target carbon materials. It is advisable to limit the ablation fluence and increase the irradiation area and pulse energy to increase the total number of ground-state carbon atoms in vacuum.

IV. PROSPECTS FOR LASER COOLING OF CARBON ATOMS

A. Deceleration rate of laser cooling using the two-photon transition

In this section, we discuss the prospects of two-photon laser cooling using ^3P - ^3D transition. The velocity change per

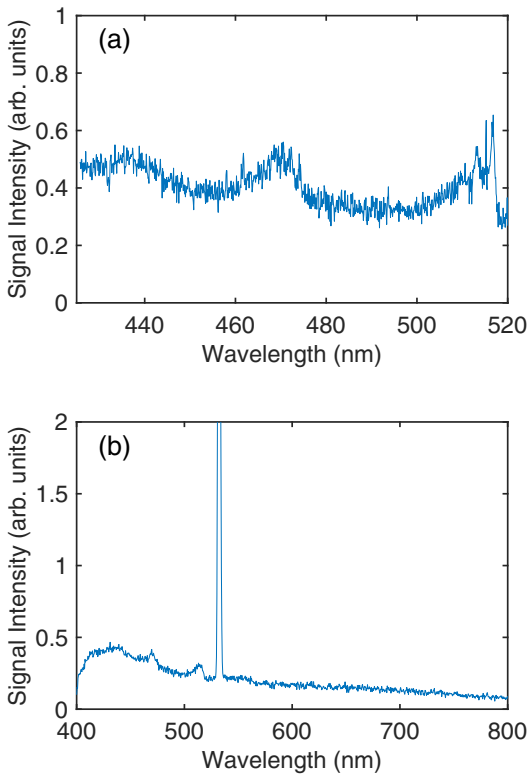

FIG. 7. Emission spectra of the surface of the HOPG sample and near the surface, at a fluence of 0.18 J/cm^2 in the wavelength ranges of (a) 425–520 nm and (b) 400–800 nm.

cooling cycle Δv is given by

$$\Delta v = \frac{2h}{m\lambda} \approx 23\,\mathrm{cm/s}, \tag{11}$$

where m is the mass of a carbon atom, λ is the photon wavelength, and h is the Planck constant. In the case of carbon, Δv is 23 cm/s, which is more than one order of magnitude greater than that of alkali metals because of the short transition wavelength and light mass of the atom. For example, in the case of rubidium 87, the velocity change per cooling cycle using the D_2 line is 6 mm/s.

When the optical intensity of the cooling laser is several GW/cm^2, which corresponds to the saturation intensity of the ^3P-^3D transition, the maximum deceleration rate is expressed as

$$\frac{\gamma}{2}\Delta v \approx 2.1 \times 10^6\,\mathrm{m/s^2}, \tag{12}$$

where γ is the decay rate from the ^3D state to the ^3P state and 18 MHz is used as its value. Considering the situation that carbon atoms with a velocity of 3000 m/s are laser cooled to a typical temperature of 100 mK at which carbon atoms can be trapped using a magnetic trap, the time required for cooling is 1.5 ms, and the distance atoms travel during that time is 3 m. However, it is not feasible to achieve such a high optical intensity (several GW/cm^2) for several milliseconds. Therefore, it is imperative that laser cooling using two-photon transition be combined with a precooling method. For example, buffer-gas cooling, which utilizes thermalization with cryogenic helium, is an established technique for precooling the beam of atoms [21]. If carbon atoms are precooled to several Kelvin, the number of cooling cycles required to introduce atoms into the magnetic trap will be reduced to approximately 100.

B. Cooling light source specialized for laser cooling of carbon atoms

A cooling light source with the corresponding pulse duration of several microseconds can realistically be constructed. In this subsection, we discuss the details of a light source suited for the laser cooling of carbon atoms. For two-photon laser cooling, both a narrow linewidth and high optical intensity are necessary. Nanosecond laser pulses cannot operate because the minimum linewidth is larger than the natural linewidth of the ^3P-^3D transition. In addition, the pulse duration was shorter than the natural decay time to the ground state after two-photon excitation. Sufficient optical intensity for effective cooling in typical continuous-wave lasers cannot be achieved. However, a pulsed laser with a pulse duration of several microseconds fulfills these requirements and will allow fast cooling in a single pulse. Such a light source can be realized by taking the third harmonic of a microsecond-pulsed laser at a wavelength of 861 nm. A Ti:sapphire pulsed laser with a long cavity photon lifetime generates microsecond pulses in the near infrared region [22]. Tunable long pulses with a bandwidth of submegahertz can be realized by conducting injection locking using a single-mode external cavity diode laser at a wavelength of 861 nm. Moreover, a pulse energy of several millijoules at a wavelength around 287 nm can be achieved by combining multipass amplification of the fundamental wave with subsequent third harmonic generation. Such a long-pulsed light source with a high pulse energy can also be utilized for the precision measurement of ^3P-^3D transition frequency by Doppler-free two-photon absorption spectroscopy and evaluation of the temperature of a cooled gas using Doppler spectroscopy.

V. CONCLUSION

In summary, we demonstrated the gas production of ground-state carbon atoms in vacuum and quantitatively evaluated the characteristics of the produced atoms, including the atomic density and velocity distribution, by observing two-photon excitation-induced fluorescence at 165.7 nm. Carbon atoms were produced by laser ablation of the HOPG target using radiation at 266 nm from the fourth harmonic of the nanosecond Q-switched Nd:YAG laser. The fluorescence at 165.7 nm was observed only upon pulsed laser irradiation at 286.9 nm, and its temporal profile was consistent with the two-step relaxation time to the ground state, proving that the fluorescence was associated with two-photon excitation on the ^3P-^3D transition. We calculated the two-photon transition rate for the ^3P-^3D transition by considering the $^3P^o$ state to be an intermediate state. We evaluated the atomic density in the excited region using the estimated two-photon transition rate and absolute signal intensity. The atomic density of the produced atoms was 6×10^9 cm^{-3} at a distance of 8 mm from the target when the fluence of the ablation laser was set to 0.18 J/cm^2, and the total number of atoms produced per pulse was estimated to be 1.5×10^8. The velocity distribution was

well fitted to the thermal Maxwell-Boltzmann distribution at a temperature of 5600 K, which is a realistic temperature for conducting laser cooling using the ^3P-^3D two-photon transition combined with buffer-gas cooling.

The emission spectral measurements of the plume indicated that a fluence of more than several J/cm^2 as used in typical laser ablation experiments is not appropriate when preparing ground-state carbon atoms to realize cold atomic gases because carbon atoms are produced at significantly high velocities, and a large number of atoms remain in highly excited electronic states with long lifetimes. For laser cooling and trapping, the thermal sublimation of graphite at low excitation fluences, where no detectable emission in the visible region can be found, is suitable for the predominant production of relatively slow carbon atoms in the ground state. It is advisable to limit the ablation fluence and increase the irradiation area and pulse energy to increase the total number of ground-state carbon atoms in vacuum.

In future work, Doppler-free two-photon absorption spectroscopy of the ^3P-^3D transition and Doppler spectroscopy for the evaluation of the temperature of cooled atoms can be realized by developing a microsecond-long intense light source at approximately 287 nm. This light source, in combination with buffer-gas cooling, can be utilized for laser cooling using the ^3P-^3D transition of the carbon atoms produced by the method demonstrated in this paper. If low-temperature carbon atoms are created, for example, chemical reactions of the molecules that make up the interstellar medium can be investigated, as demonstrated using monovalent carbon ions [23].

ACKNOWLEDGMENTS

This work was supported by Japan Science and Technology Agency Precursory Research for Embryonic Science and Technology (Grant No. JPMJPR190B) and Ministry of Education, Culture, Sports, Science, and Technology Quantum Leap Flagship Program (Grant No. JPMXS0118067246).

APPENDIX A: DEVIATION OF EQ. (2)

To obtain the fitting curve given in Eq. (2), we assume that the carbon atoms are produced as a one-dimensional beam. Then, the velocity distribution of the produced atoms $f(v)$ is given as [24]

$$f(v)dv = 2N\left(\frac{m}{2k_BT}\right)^2 v^3 \exp\left(-\frac{mv^2}{2k_BT}\right)dv, \tag{A1}$$

where T is the temperature and m is the mass of produced atoms. N is the total number of produced atoms, and $f(v)$ is normalized to satisfy $\int_0^\infty f(v)dv = N$. As the atomic density is sufficiently low (6×10^9 cm^{-3}), we assume that the produced atoms maintain their initial velocities throughout their flight. Then, the relation between the velocity v and arrival time t at a travel distance of L is expressed as

$$vt = L. \tag{A2}$$

Since v and t are related through Eq. (A2), we can derive the arrival time distribution of produced atoms from their velocity distribution. Using $v = \frac{L}{t}$ and $dv = -\frac{L}{t^2}dt$, we perform a variable conversion as follows:

$$f(v)dv = f\left(\frac{L}{t}\right)\left(-\frac{Ldt}{t^2}\right) \equiv F(t)(-dt). \tag{A3}$$

Here, we defined the arrival time distribution $F(t)$ so that the sign of $F(t)$ is consistent with the direction of change in the velocity and arrival time. From Eq. (A3), $F(t)$ is expressed as

$$F(t) = \frac{2N}{t^5}\left(\frac{mL^2}{2k_BT}\right)^2 \exp\left(-\frac{mL^2}{2k_BTt^2}\right). \tag{A4}$$

By replacing $2N(\frac{mL^2}{2k_BT})^2$ with a constant A, we obtain Eq. (2).

APPENDIX B: EVALUATION OF THE NUMBER OF ATOMS PRODUCED

To obtain the total number of ground-state carbon atoms N produced per ablation pulse using the derived atomic density, we assumed that the carbon atoms were produced instantaneously and uniformly in the irradiated area on the sample surface. The beam diameter of the ablation pulse was 1.5 mm on the sample surface, which was non-negligible compared to the distance between the surface and detection position (8 mm). Therefore, we assumed that all the produced atoms traveled to the surface normal. Here, we considered the center of the ablation beam on the surface as the origin. The sample surface was the xy plane, and the surface normal was the z axis. Then, the velocity components of the produced atoms in the x and y directions were $v_x = 0$ and $v_y = 0$. Denoting the velocity component in the z direction as v_z, the velocity distribution of the produced beam of carbon atoms $f(v_z)$ is

$$f(v_z) = 2N\left(\frac{m}{2k_BT}\right)^2 v_z^3 \exp\left(-\frac{mv_z^2}{2k_BT}\right), \tag{B1}$$

where $f(v_z)$ is normalized to satisfy $\int_0^\infty f(v_z)dv_z = N$. As the travel distance of atoms after t_0 from the gas production is represented by v_zt_0, the atomic density $n(x, y, z; t)$ at $t = t_0$ can be expressed as

$$n(x, y, z; t = t_0) = \begin{cases} 0 & (x^2 + y^2 > l^2) \\ \frac{2N}{\pi l^2}\left(\frac{m}{2k_BTt_0^2}\right)^2 z^3 \exp\left(-\frac{mz^2}{2k_BTt_0^2}\right) & (x^2 + y^2 \leqslant l^2, z \geqslant 0) \\ 0 & (z < 0), \end{cases} \tag{B2}$$

where $n(x, y, z; t = t_0)$ was normalized to satisfy $\int n(x, y, z; t = t_0)dxdydz = N$, and l is the beam radius of the ablation laser on the sample surface. Because the atomic density at $z = 8$ mm, $T = 5600$ K, and $t_0 = 2.5$ μs is 6×10^9 cm^{-3}, we obtain the following equation:

$$N \times (40\,\text{cm}^{-3}) = 6 \times 10^9\,\text{cm}^{-3}, \tag{B3}$$

$$N = 1.5 \times 10^8. \tag{B4}$$

Therefore, the total number of ground-state atoms N produced per ablation pulse is 1.5×10^8. Note that the total number of atoms derived here is an underestimate, because the carbon atoms produced travel with an angular spread from the surface normal direction. We must measure the angular distribution to estimate N more precisely.

[1] M. H. Anderson, J. R. Ensher, M. R. Matthews, C. E. Wieman, and E. A. Cornell, Science **269**, 198 (1995).
[2] M. Greiner, O. Mandel, T. Esslinger, T. W. Hänsch, and I. Bloch, Nature (London) **415**, 39 (2002).
[3] S. A. Diddams, T. Udem, J. C. Bergquist, E. A. Curtis, R. E. Drullinger, L. Hollberg, W. M. Itano, W. D. Lee, C. W. Oates, K. R. Vogel *et al.*, Science **293**, 825 (2001).
[4] H. Katori, M. Takamoto, V. G. Pal'chikov, and V. D. Ovsiannikov, Phys. Rev. Lett. **91**, 173005 (2003).
[5] S. Schmid, A. Härter, and J. H. Denschlag, Phys. Rev. Lett. **105**, 133202 (2010).
[6] T. W. Hijmans, O. J. Luiten, I. D. Setija, and J. T. M. Walraven, J. Opt. Soc. Am. B **6**, 2235 (1989).
[7] I. D. Setija, H. G. C. Werij, O. J. Luiten, M. W. Reynolds, T. W. Hijmans, and J. T. M. Walraven, Phys. Rev. Lett. **70**, 2257 (1993).
[8] M. Allegrini and E. Arimondo, Phys. Lett. A **172**, 271 (1993).
[9] D. Kielpinski, Phys. Rev. A **73**, 063407 (2006).
[10] A. M. Jayich, X. Long, and W. C. Campbell, Phys. Rev. X **6**, 041004 (2016).
[11] T. Sakamoto and K. Yoshioka, Opt. Lett. **46**, 4642 (2021).
[12] F. Kokai and Y. Koga, Nucl. Instrum. Methods Phys. Res., Sect. B **121**, 387 (1997).
[13] H. C. Ong and R. P. H. Chang, Phys. Rev. B **55**, 13213 (1997).
[14] P. Das, G. S. Ondrey, N. Van Veen, and R. Bersohn, J. Chem. Phys. **79**, 724 (1983).
[15] K. H. Becker, K. J. Brockmann, and P. Wiesen, J. Chem. Soc. Faraday Trans. 2 **84**, 455 (1988).
[16] M. Aldén, P. E. Bengtsson, and U. Westblom, Opt. Commun. **71**, 263 (1989).
[17] H. Bergström, H. Hallstadius, H. Lundberg, and A. Persson, Chem. Phys. Lett. **155**, 27 (1989).
[18] A. Kramida, Yu. Ralchenko, J. Reader, and NIST ASD Team, NIST Atomic Spectra Database (ver. 5.9), National Institute of Standards and Technology, Gaithersburg, MD, 2021, https://physics.nist.gov/asd [27 June 2022].
[19] S. Sinha, J. Laser Appl. **30**, 012008 (2018).
[20] R. J. Papoular and R. Papoular, Mon. Notices Royal Astron. Soc. **443**, 2974 (2014).
[21] R. deCarvalho, J. M. Doyle, B. Friedrich, T. Guillet, J. Kim, D. Patterson, and J. D. Weinstein, Eur. Phys. J. D **7**, 289 (1999).
[22] K. Yamada, Y. Tajima, T. Murayoshi, X. Fan, A. Ishida, T. Namba, S. Asai, M. Kuwata-Gonokami, E. Chae, K. Shu *et al.*, Phys. Rev. Appl. **16**, 014009 (2021).
[23] T. Yang, A. Li, G. K. Chen, Q. Yao, A. G. Suits, H. Guo, E. R. Hudson, and W. C. Campbell, Sci. Adv. **7**, eabe4080 (2021).
[24] C. J. Foot, *Atomic Physics* (Oxford University, New York, 2007), p. 152.